ROWAN UNIVERSITY **2016**

Validation of SunCell Technology

Valuator:
K.V. Ramanujachary
Professor
Department of Chemistry and Biochemistry
Rowan University, Glassboro, NJ, 08028

Submitted to
Brilliant Light Power, Inc.

K.V. Ramanujachary

Evaluator's Signature: Date: May 16, 2016

BRILLIANT LIGHT POWDER SUN-CELL VALIDATION (April-May 2016)

The present report deals with validation studies of four new experiments carried out by the scientists at Brilliant Light Power, Inc. at their Cranbury, NJ laboratories in my presence. The results presented here have been witnessed by the evaluator and all the measurement and experimental protocols employed by Brilliant Light Power are scientifically sound. In essence, by applying high current and modestly low voltages to metal/metal composites in moist environments, the Brilliant Light Power company has achieved what amounts to a breakthrough in low-cost energy generation. The technology described by the Brilliant Light Power uses eco-friendly chemicals that are relatively inexpensive and renewable. With proper design and additional developmental work, the technology could be engineered to build inexpensive commercial power generators that use H_2O as fuel.

While the mechanism responsible for the generation of power seems to be common to all the four experiments, for the sake of clarity each one of these are dealt separately in the following sections.

A. Sun-Cell Thermal Burst Power Measurement:

In this demonstration, small amount of (~1mol% or 0.5 mole%) was allowed to react with molten silver in an atmosphere of 3% hydrogen and 97% Ar. The difference in the input and output energies were measured accurately both before and after the addition of to illustrate the dramatic effect of addition to the molten silver. The total input power was calculated based on the slopes of the temporal coolant temperature that was in thermal contact with the reaction zone.
Figures A.1 and A.2 show the design of the instrumentation in which 700g of the molten silver is placed in a 100mL plasma reaction chamber. To melt the silver, the reaction chamber is heated by commercial inductive heater operating at 30KHz heating power and a cold jacket. An electromagnetic pump is used to inject molten silver to the electrodes (the addition was done manually) that are powered by super capacitors.

The input power measurement for each of the inductively coupled heater and the electrodes was measured with a digital oscilloscope. To calculate the power, the voltages of the oscilloscope were multiplied with the acquired current and were divided by the duration of the run. The power consumed by the electromagnetic pump used for guiding the molten silver near the electrodes was determined using the current and voltage values obtained from the oscilloscope.

The results demonstrated the feasibility of obtaining nearly 1.5 million watts of power when using an input power of just 8.6 kW. The experimental methods and results are summarized below.

Figure 1: SunCell® showing electrode penetrations on opposite sides, internal electromagnetic pump (EM) nozzle, electrodes and water cooled bus bars, water cooled inductively coupled heater coil inside insulation, and electrode EM pump magnets.

A schematic of the Suncell is shown in Fig. 2.

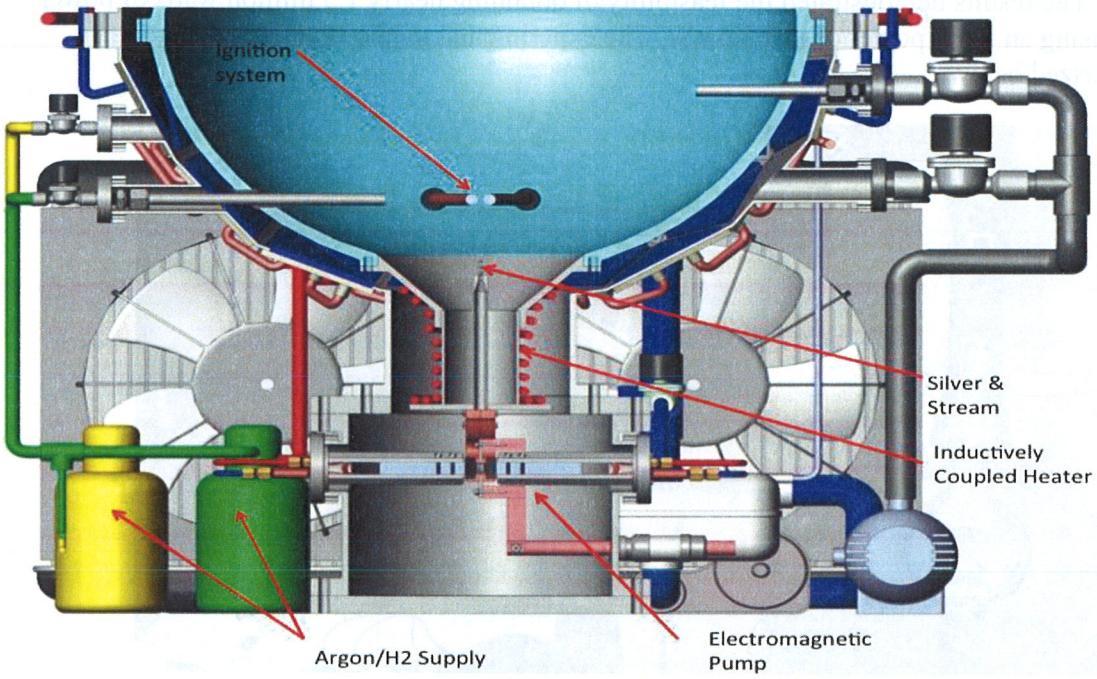
Ignition system
Silver & Stream
Inductively Coupled Heater
Argon/H2 Supply
Electromagnetic Pump

Fig.2- A design of the Suncell showing the overall design of a working unit.

Results and Discussion:

Fig.3 shows the results of the test of addition of 1 mole% ;) to molten silver with 9 liter per min 97%Ar/3% H_2 for test 042016DR. The input powers were (i) inductively coupled heater (3.5 kW), (ii) electrodes (3.5 kW), and (iii) EM pump (540 W), totaling 7540 W. The reaction initiated at first time point of line 2 with the commencement of the liquid metal injection and plasma ignition wherein supplied the oxygen to form HOH catalyst. From the curve fits of the coolant thermal response as a function of time, the ratio of the pre-ignition (line 1) and post ignition (line 2) temporal thermal responses was 82,080/137 = 599. Using the sum of the heater and pump powers of 4300 W being the initial constant input power, the corresponding post reaction initiation power was 2,576,000 W wherein the additional electrode power contribution of 3.5 kW was trivial. One mole% was added at the first time point of line 3 wherein the total constant input power was 7540 W. The pre-addition slope is approximated as the initial slope of 137 corrected by added electrode power, 137 X [7540/4300] = 240. The ratio of the pre-addition and post addition temporal thermal responses is 23,330/240 = 97 corresponding to a post oxygen source addition power of 731,000 W. The reduction of can provide a trivial power as shown in Sec. III. The reaction abruptly terminated when the wall comprising high temperature SS of 0.148" (3.7 mm) thickness melted and the silver leaked out. Representative images of SunCells® post meltdown are shown in Figure 4. In a commercial SunCell®, refractory materials such as tungsten (°C) replace high-temperature stainless steel (M.P. 1500 °C) in order to achieve the high temperatures capable of incandescent emission to a photovoltaic converter of the corresponding light to electricity.

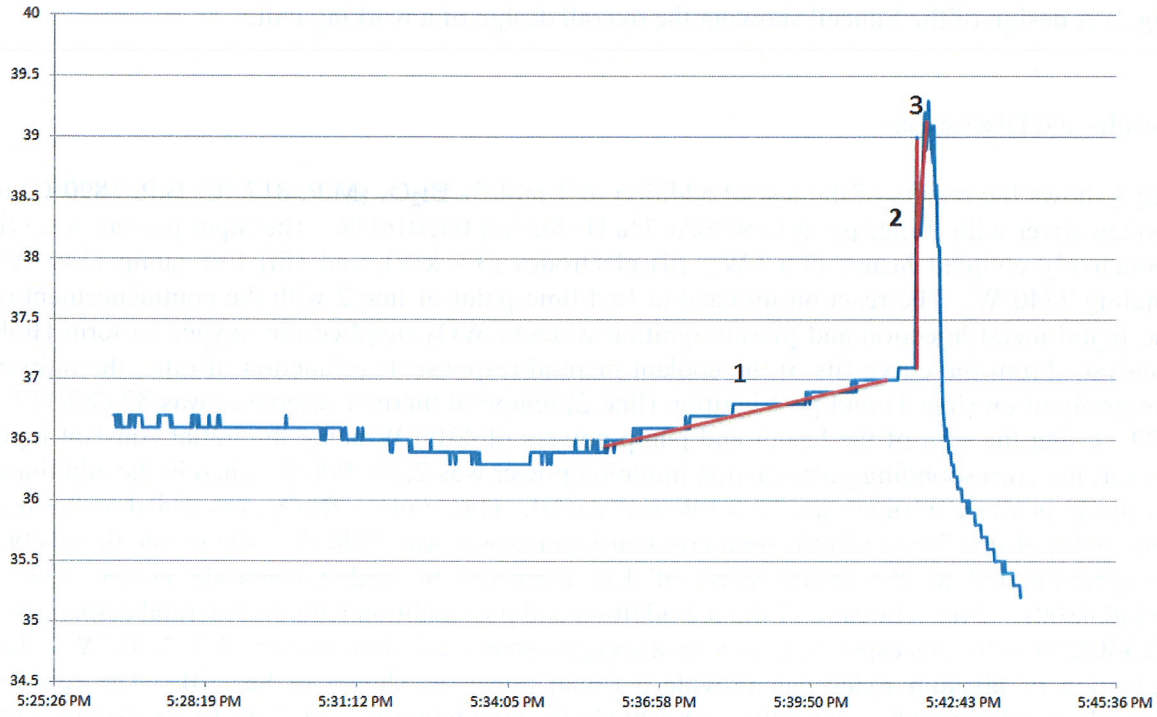

Figure 3. 042016DR test of addition of 1 mole% to molten silver with 9 liter per min 97%Ar/3%H_2 showing the temperature of the water in the antenna coil cooling loop of the inductively coupled heater as a function of time. The coolant thermal responses as a function of time for different experimental regimes were curve fit for thermal power determination: line 1 is the curve fit of the initial non-reaction period; line 2 is the curve fit of the reaction period following plasma initiation; line 3 is the curve fit of the reaction period post addition of

(A)

(B)

(C)

Figure 4A-C. Images of SunCells® that underwent meltdown in about 10 s due to the extraordinary power generated in the reactor. The inductively coupled heater coolant coil was splayed open in the melted section for visualization. A. Test 042616JL. B. Test 0505126ADR. C. Test 050516BDR.

The results of the test of addition of 1 mole% to molten silver with 9 liter per min 97%Ar/3%H_2 for test 042616ADR are shown in Figure 5. The input powers were (i) inductively coupled heater (4 kW), (ii) electrodes (3.6 kW for line 2 and 3.5 kW for line 3), and (iii) EM pump (800 W), totaling 8300 W. The WO_3-supported reaction initiated at first time point of line 2 with the commencement of the liquid metal injection and plasma ignition. From the curve fits of the coolant thermal response as a function of time, the ratio of the pre-ignition (line 1) and post ignition (line 2) temporal thermal responses was 14,700/420 = 35. Using the sum of the heater and pump powers of 4800 W as the initial constant input power, the corresponding post reaction initiation power was 168,000 W wherein the additional electrode power contribution of 3.6 kW was trivial. One mole% was added at the first time point of line 3 wherein the total constant input power was 8300 W. The pre-addition slope is approximated as the initial slope of 420 corrected by added electrode power, 420 X [8300/4800]= 726. The ratio of the pre-addition and post addition temporal thermal responses is 86,400/726 = 119 corresponding to a post oxygen source addition power of 987,700 W. The reduction of can provide a trivial power as described in Sec. III. The reaction abruptly terminated when the wall comprising high temperature SS of 0.148" (3.7 mm) thickness melted and the silver leaked out.

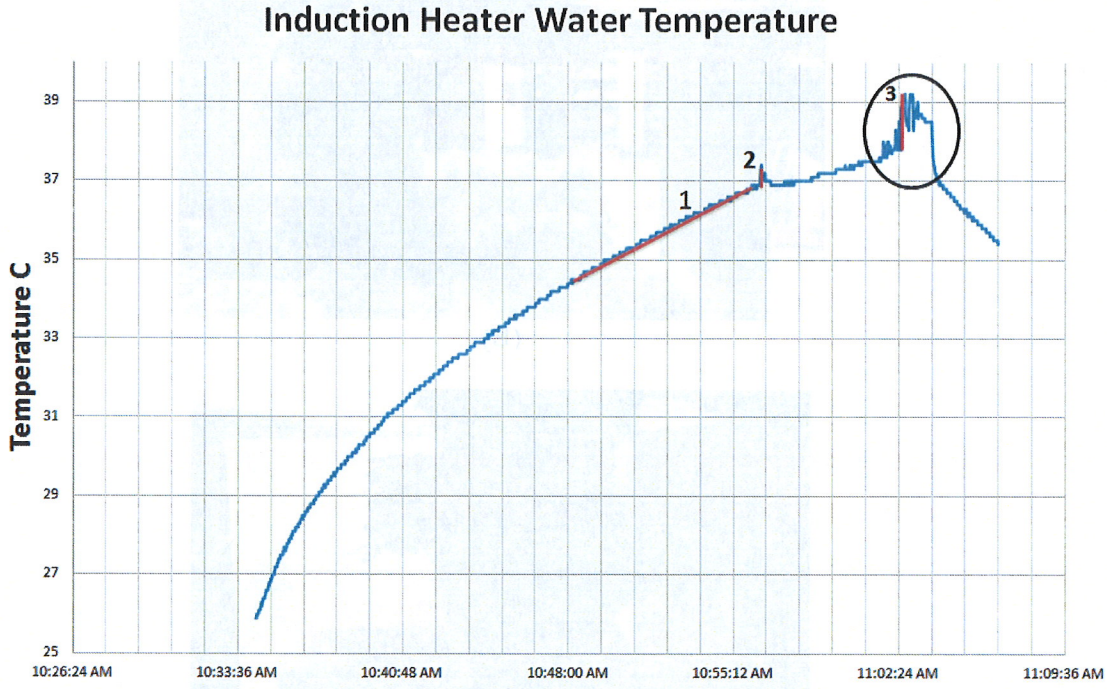

Figure 5. 042616ADR test of addition of 1 mole% to molten silver with 9 liter per min 97%Ar/3%H_2 showing the temperature of the water in the antenna coil cooling loop of the inductively coupled heater as a function of time. The coolant thermal responses as a function of time for the different experimental regimes were curve fit for thermal power determination: line 1 is the curve fit of the initial non-reaction period; line 2 is the curve fit of the reaction period following plasma initiation; line 3 is the curve fit of the reaction period post addition of .

The results of the test of addition of 1 mole% to molten silver with 9 liter per min 97%Ar/3%H_2 for test 042616BDR are shown in Figure 6. The input powers were (i) inductively coupled heater (4 kW), (ii) electrodes (3.6 kW), and (iii) EM pump (800 W), totaling 8400 W. The -supported reaction initiated at first time point of line 2 with the commencement of the liquid metal injection and plasma ignition. From the curve fits of the coolant thermal response as a function of time, the ratio of the pre-ignition (line 1) and post ignition (line 2) temporal thermal responses was 17,280/321 = 53.8. Using the sum of the heater and pump powers of 4800 W as the initial constant input power, the corresponding post reaction initiation power was 258,240 W wherein the additional electrode power contribution of 3.5 kW was trivial. One mole% was added at the first time point of line 3 wherein the total constant input power was 8400 W. The pre-addition slope is approximated as the initial slope of 321 corrected by added electrode power, 321 X [8400/4800] = 562. The ratio of the pre-addition and post addition temporal thermal responses is 8537/562 = 15 corresponding to a post oxygen source addition power of 126,000 W. The reduction of can provide a trivial power as shown in Sec. III. The reaction abruptly terminated when the wall comprising high temperature SS of 0.148" (3.7 mm) thickness melted and the silver leaked out.

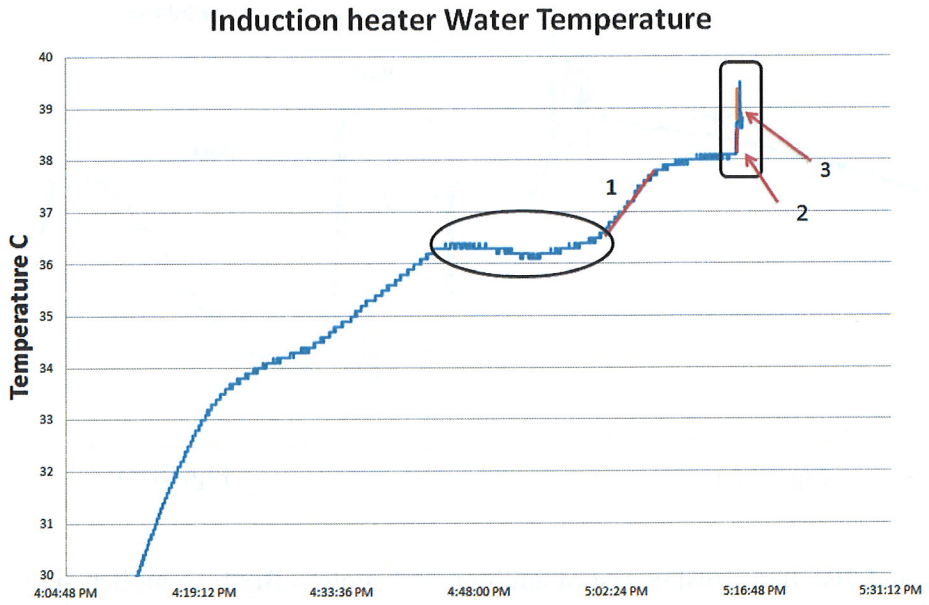

Figure 6. 042616BDR test of addition of 1 mole% to molten silver with 9 liter per min 97%Ar/3%H_2 showing the temperature of the water in the antenna coil cooling loop of the inductively coupled heater as a function of time. The coolant thermal responses as a function of time for the different experimental regimes were curve fit for thermal power determination: line 1 is the curve fit of the initial non-reaction period; line 2 is the curve fit of the reaction period following plasma initiation; line 3 is the curve fit of the reaction period post addition of . Additional solid silver as added and melted at the circled time zone since the electromagnetic pump tube filled corresponding to a drop in the molten silver level.

The results of the test of addition of 1 mole% to molten silver with 9 liter per min 97%Ar/3%H_2 for test 042716BDR are shown in Figures 7A and 7B. The input powers were (i) inductively coupled heater (4 kW), (ii) electrodes (4.9 kW), and (iii) EM pump (800 W), totaling 9700 W. The -supported reaction initiated at point 1 (Figures 7A and 7B) with the commencement of the liquid metal injection and plasma ignition. One mole% was added at the point 2 (Figure 7B) wherein the total constant input power was 9700 W. The pre-addition slope is approximated as the initial slope 1 of 135 (Figure 7A) corrected by electrode power added to the sum of the heater and pump powers of 4800 W as the initial constant input power, 135 X [9700/4800] = 273. The ratio of the pre-addition and post addition temporal thermal responses is 146900/273 = 538 corresponding to a post oxygen source addition power of 5,220,000 W. As shown in Figure 7B, the addition thermal burst was followed by another and then a sustained thermal event. The curve fit is given by line 3 having a slope of 4420 corresponding a relative slope of 4420/273 = 16 and a power of 155,200 W. The reduction of can provide a trivial power as shown in Sec. III. The reaction abruptly terminated when the wall comprising high temperature SS of 0.148" (3.7 mm) thickness melted and the silver leaked out.

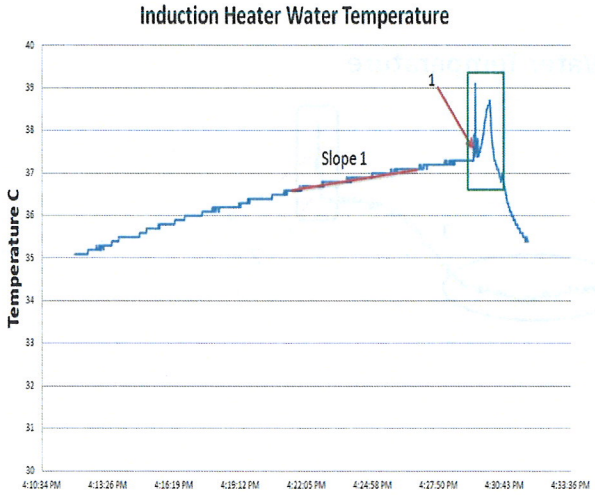

Fig. 7(A)

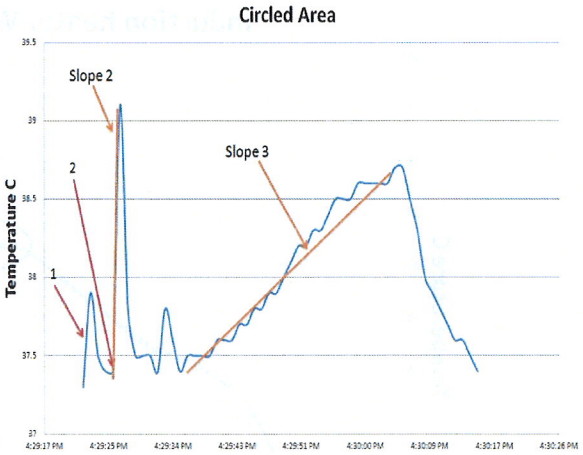

Fig. 7(B)

Figures 7A and 7B. 042616BDR test of addition of 1 mole% to molten silver with 9 liter per min 97%Ar/3%H_2 showing the temperature of the water in the antenna coil cooling loop of the inductively coupled heater as a function of time. The coolant thermal responses as a function of time for the different experimental regimes were curve fit for thermal power determination. (A) Line 1 is the curve fit of the initial non-reaction period and point 1 is the initiation of the plasma reaction. (B) Expansion of the boxed section of the response shown in Figure 7A wherein point 1 is the initiation of the plasma reaction; point 2 is the addition time point of , line 2 is the curve fit of the initial reaction period post addition of ; line 3 is the curve fit of the reaction period post addition of showing a more sustained thermal event.

The results of the test of addition of 0.5 mole% to molten silver with 9 liter per min 97%Ar/3%H_2 for test 042616JL are shown in Figure 8. In this case, rather than using the thermal response of the inductively coupled heater coolant loop which was not well coupled to the cell, the power due to the hydrino reaction at plasma initiation and at addition was determined using the combined coolant lines from the magnets of electromagnetic pump and the electrode bus bars. The input powers were (i) inductively coupled heater (2.6 kW), (ii) electrodes (5.6 kW), and (iii) EM pump (460 W), totaling 8660 W. The reaction consistently initiated at point 3 with the commencement of the liquid metal injection and plasma ignition wherein supplied the oxygen to form HOH catalyst. From the curve fits of the coolant thermal response as a function of time, the ratio of the pre-ignition slope at point 1 and post ignition slope at point 3 was 93/1.6 = 58. Using the sum of the heater and pump powers of 3060 W as the initial constant input power, the corresponding post reaction initiation power was 177,480 W wherein the additional electrode power contribution of 5.6 kW was trivial. 0.5 mole% was added at the point 4 wherein the total constant input power was 8660 W. The pre-addition slope is approximated as the initial slope of 1.6 corrected by added electrode power, 1.6 X [8660/3060] = 2.8. Using the slope at the high power point 5 wherein the high temperature SS of 0.148" (3.7 mm) thickness melted and the silver leaked out, the ratio of the pre-addition and post addition temporal thermal responses is 508/2.8 = 181 corresponding to a post oxygen source addition power of 1,567,000 W. The reduction of can provide a trivial power as shown in Sec. III. The reaction abruptly terminated when the wall comprising high temperature SS of 0.148" (3.7 mm) thickness melted and the silver leaked out (Figure 4A).

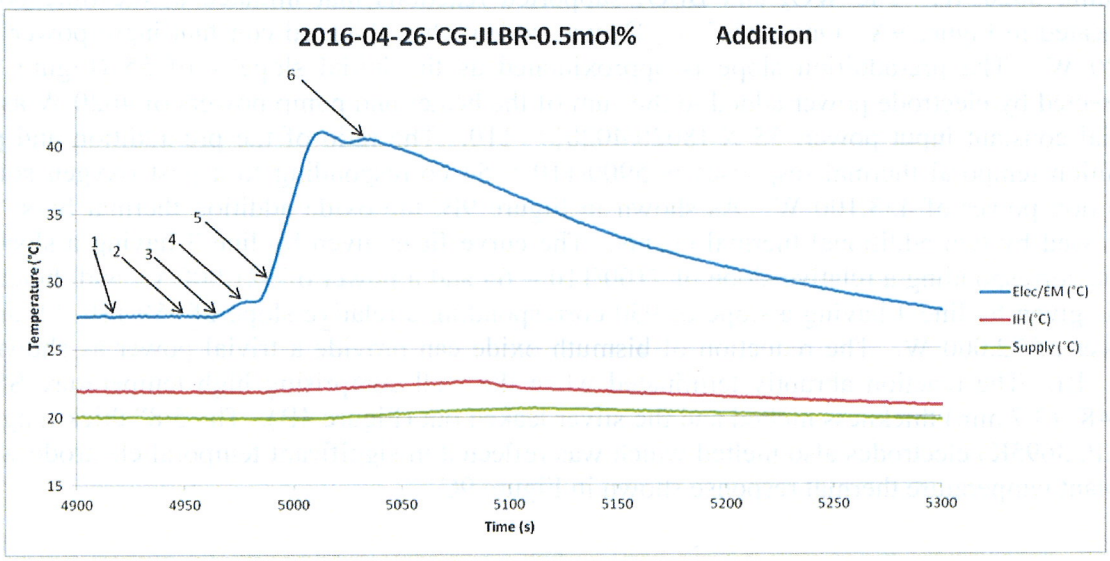

Figure 8. 042616JL test of addition of 0.5 mole% to molten silver with 9 liter per min 97%Ar/3%H_2 showing the temperature of the water in the EM pump and bus bars cooling loop as a function of time. The coolant thermal responses as a function of time for the different experimental regimes were curve fit for the thermal power determination. The regimes and corresponding slopes are given in Table 1. The inductively coupled heater coolant loop was not thermally coupled to the cell in this run.

Table 1. Experimental regimes and corresponding slopes of the coolant thermal response for the 042616JL test.

Event	Slope Ahead (mK/s)	EM Pump Power	IH Pump Power	Electrode Power	Regimes
1	0.437	0.60 kW	2.6 kW	NA	Only EM pumping and heating was active during this period
2					Start of first burst of pumping and electrode firing
2A		0.46 kW Time Average Over the Run Duration	2.6 kW Time Average Over the Run Duration	5.6 kW Time Average Over the Run Duration	Only EM pumping and heating was active during this period
3	94.313				Start of strong sustained pumping and electrode firing
4	10.418				0.5 mole% added; no significant change in waveform; ~9L/min 3% H2:Ar added within ~3s
5	516.623				End of strong run, wall may have melted here, weaker run and waveform
6					Weaker burst ended, end of run, end of waveform
					NOTE: Pumping, electrodes and heating were active for all Events except Events 1 and 2A

The results of the test of addition of 1 mole% to molten silver with 9 liter per min 97%Ar/3%H_2 for test 0505ADR are shown in Figures 9A-C. The input powers were (i) inductively coupled heater (3.22 kW), (ii) electrodes (4 kW), and (iii) EM pump (800 W), totaling 8020 W. The and supported reactions that initiated at the time points indicated in Figure 9A. One mole% was added when the total constant input power was 8020 W. The pre-addition slope is approximated as the initial slope 1 of 55 (Figure 9A) corrected by electrode power added to the sum of the heater and pump powers of 4020 W as the initial constant input power, 55 X [8020/4020] = 110. The ratio of the pre-addition and post addition temporal thermal responses is 5900/110 = 54 corresponding to a post oxygen source addition power of 433,100 W. As shown in Figure 9B, the oxide addition thermal burst was followed by two additional thermal events. The curve fit is given by line 3 having a slope of 7100 corresponding a relative slope of 7100/110 = 65 and a power of 521,000 W, and the curve fit is given by line 4 having a slope of 950 corresponding a relative slope of 950/110 = 9 and a power of 72,000 W. The reduction of can provide a trivial power as shown in Sec. III. The reaction abruptly terminated when the wall comprising high temperature SS of 0.148" (3.7 mm) thickness melted and the silver leaked out (Figure 4B). The 5/8" thick tungsten (M.P. 3695K) electrodes also melted which was reflected in significant temporal electrode water coolant temperature thermal response shown in Figure 9C.

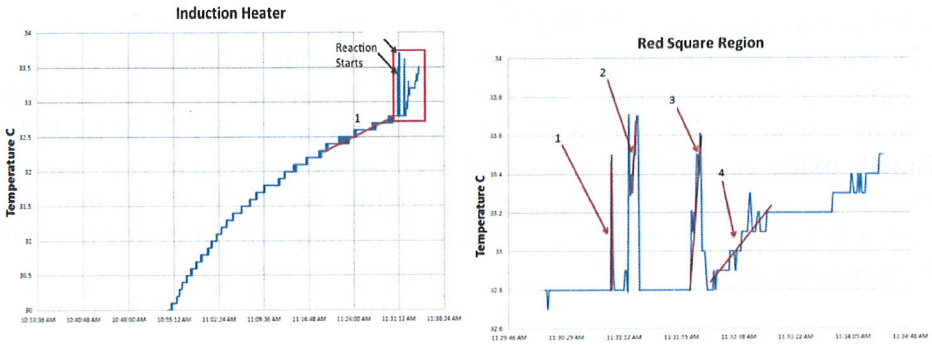

(A) (B)

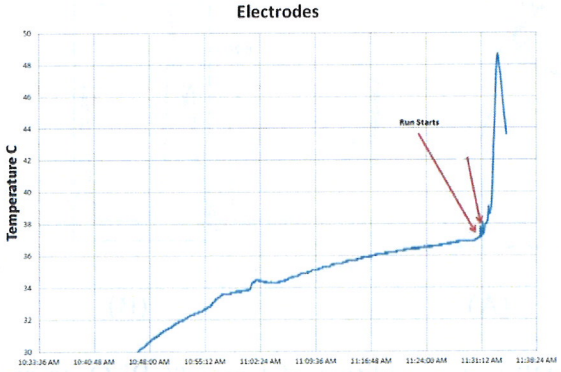

(C)

Figures 9A-C. 050516ADR test of addition of 1 mole% to molten silver with 9 liter per min 97%Ar/3%H_2 showing the temperature of the water in the antenna coil cooling loop of the inductively coupled heater as a function of time. The coolant thermal responses as a function of time for the different experimental regimes were curve fit for thermal power determination. (A) Line 1 is the curve fit of the initial non-reaction period; the time points of reaction initiation and addition are indicated. (B) Expansion of the boxed section of the response shown in Figure 9A wherein line 1 corresponds to the cure fit of the initiation of the plasma reaction; line 2 is the curve fit of the initial reaction period post addition of ; lines 3 and 4 are the curve fits of the reaction period post addition of showing two more thermal events. (C) The temporal electrode water coolant temperature thermal response showing a significant slope change after addition wherein the heavy W electrodes melted and the silver vaporized at about the pumping rate of 2.5 ml/s.

The results of the test of addition of 1 mole% to molten silver with 9 liter per min 97%Ar/3% for test 0505BDR are shown in Figures 10A and 10B. The input powers were (i) inductively coupled heater (3.65 kW), (ii) electrodes (6 kW), and (iii) EM pump (800 W), totaling 10,450 W. The and supported hydrino reactions initiated at the time points indicated in Figure 10A. One mole% was added when the total constant input power was 10,450 W. The pre-addition slope is approximated as the initial slope 1 of 118 (Figure 10A) corrected by electrode power added to the sum of the heater and pump powers of 4450 W as the

initial constant input power, 118 X [10,450/4450] = 277. The ratio of the pre-addition and post addition temporal thermal responses is 7344/277 = 27 corresponding to a post oxygen source addition power of 282,150 W. As shown in Figure 10B, the addition thermal burst was followed by an additional thermal event. The curve fit is given by line 3 having a slope of 16,400 corresponding a relative slope of 16,400/110 = 149 and a power of 1,557,000 W. The reduction of can provide a trivial power as shown in Sec. III. The reaction abruptly terminated when the wall comprising high temperature SS of 0.148" (3.7 mm) thickness melted and the silver leaked out (Figure 4C). The 5/8" thick tungsten (M.P. 3695K) electrodes also melted and welded together.

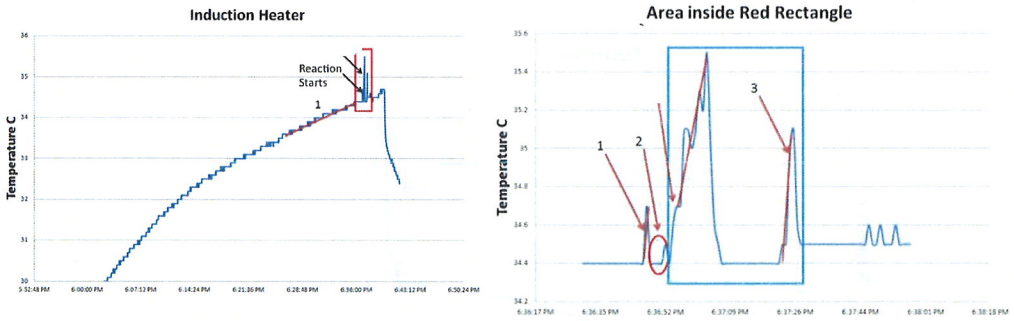

(A) (B)

Figures 10A-B. 050516BDR test of addition of 1 mole% to molten silver with 9 liter per min 97%Ar/3%H_2 showing the temperature of the water in the antenna coil cooling loop of the inductively coupled heater as a function of time. The coolant thermal responses as a function of time for the different experimental regimes were curve fit for thermal power determination. (A) Line 1 is the curve fit of the initial non-reaction period; the time points of reaction initiation and addition are indicated. (B) Expansion of the boxed section of the response shown in Figure 10A wherein line 1 corresponds to the curve fit of the initiation of the plasma reaction; line 2 is the curve fit of the initial reaction period post addition of ; line 3 is the curve fit of the reaction period post addition of showing an additional thermal event; point 2 corresponding to a point where there was a short pause in ignition current due to injection alignment.

The reduction of can provide a trivial power contribution of less than 18.6 W as shown in Sec III. With addition, the observed reaction powers of 731,000 W, 987,700 W, 126,000 W, 5,220,000 W, 1,567,000 W, 433,100 W, and 282,150 W were of the same magnitude as those recorded by absolute spectroscopy over the wavelength region 5-800 nm (McPherson 0.2 meter monochromator Model 302, Seya-Namioka type equipped with a 1200 lines/mm holographic grating with a platinum coating; McPherson grazing incidence EUV spectrometer Model 248/310G equipped with a platinum-coated 600 g/mm or a platinum-coated 1200 g/mm grating; Andor iDus CCD detector cooled to -60 °C; Mightex spectrometer) and measured by calorimetry using a commercial bomb calorimeter (Parr 1341).

III. Theoretical Chemical Power

The standard thermodynamic parameters for the most exothermic chemical reaction for silver, , and hydrogen corresponding to the addition of to molten silver with the flowing hydrogen gas are given in Table 2. The cell gas was 9 liters/min $Ar/H_2(3\%)$; so, hydrogen comprised the limiting reagent for power production. The limiting hydrogen was flowed at 2×10^{-4} moles H_2/s corresponding to a maximum power of 18.6 W.

Table 2. Thermodynamic parameters (1400 K) of the reaction of and H_2O to form

Reaction	+ →			
	H2O		H2	
Stoichiometry	2	3	1	3
$\Delta_f H$ (kJ/mol)	41.780	-197.759	-330.697	33.250
S (J/(K*mol))	120.102	248.361	439.718	176.768
H (kJ/mol)	83.560	-593.277	-330.697	99.750
G (kJ/mol)	-252.726	-1636.393	-946.302	-642.676
T (K)	1400			
n	3			
Results per mol:				
ΔHrxn (kJ/mol	139.385			
ΔGrxn (kJ/mol	150.071			
E°rxn (1400 K)	-1.037	Volts		

Specifically, a red heat, reacts with water to form the

+ → +

(https://www.webelements.com

is a regenerative oxygen source for a commercial design. Another candidate that has similar power performance with no theoretical power contribution is (

IV. Heat Transfer Analysis to Determine the Effect of the Addition of a Power Source

The liquid-cooled cell body (CB) has mass M, heat capacity C and temperature T_{CB}, cf. Figure 9. Coolant, with specific heat C_p, flows into the CB at steady flow rate m and constant inlet temperature T_{Inlet}. Initially, $t \le 0$, the energy input rate q to the CB is zero so that the CB and the coolant are isothermal at the coolant inlet temperature: $T_{CB} = T_{Exit} = T_{Inlet}$. Consider a step jump in energy input rate from $q = 0$ to $q = Q$ for $t > 0$:

$$t \le 0: \quad q = 0, \quad T_{CB} = T_{Inlet} = T_{Exit}$$

$$t > 0: \quad q = Q, \quad T_{CB} = T_{CB}(t), \quad T_{Exit} = T_{Exit}(t)$$

Figure 9. CB thermal model

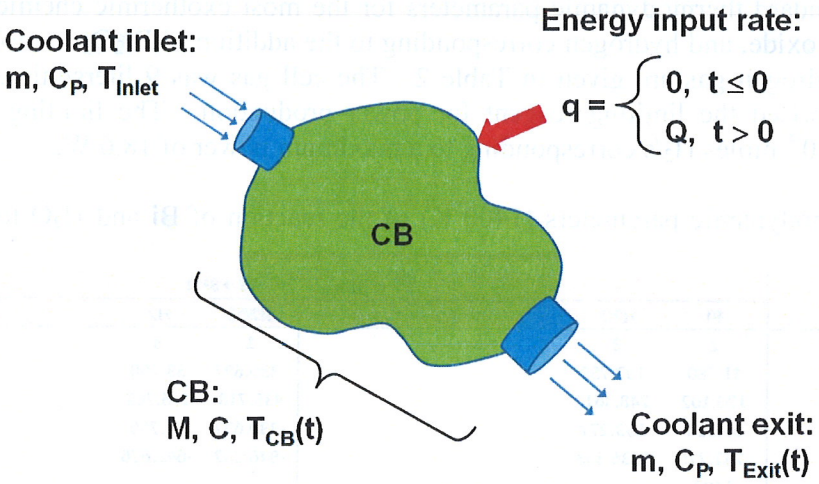

Conservation of energy for the CB for times $t > 0$ requires

$$\frac{dE_{CB}(t)}{dt} = mC_P\left(T_{Inlet} - T_{Exit}(t)\right) + Q$$

The internal energy of the CB is

$$E_{CB}(t) = MC\left(T_{CB}(t) - T_0\right)$$

where T_0 is a reference temperature. Assume that the average temperature of the CB at any time is the mean value of the inlet and exit cooling water stream temperatures:

$$T_{CB}(t) = \frac{T_{Inlet} + T_{Exit}(t)}{2}$$

Then

$$\frac{MC}{2}\frac{dT_{Exit}(t)}{dt} = mC_P\left(T_{Inlet} - T_{Exit}(t)\right) + Q$$

$$\frac{MC}{2}\frac{dT_{Exit}(t)}{\left[mC_P\left(T_{Inlet} - T_{Exit}(t)\right) + Q\right]} = dt$$

$$-\frac{MC}{2mC_P}\, d\log\left[mC_P\left(T_{Inlet} - T_{Exit}(t)\right) + Q\right] = dt$$

Integrating using $T_{Exit}(0) = T_{Inlet}$

$$\log\{mC_P(T_{Inlet}-T_{Exit}(t))+Q\}-\log\{Q\}=-\frac{2mC_p}{MC}t$$

$$\log\left\{\frac{mC_P(T_{Inlet}-T_{Exit}(t))+Q}{Q}\right\}=-\alpha t,\quad \alpha=\frac{2mC_p}{MC}$$

The coolant temperature rise, cf. Figure 10, is

$$T_{Exit}(t)-T_{Inlet}=\frac{Q}{mC_p}\left(1-e^{-\alpha t}\right)$$

The rate of coolant temperature increase at any time t is

$$\frac{dT_{Exit}(t)}{dt}=\frac{Q\alpha}{mC_p}e^{-\alpha t}$$

and the maximum rate occurs at time t = 0:

$$\left(\frac{dT_{Exit}(t)}{dt}\right)_{Max}=\frac{Q\alpha}{mC_P}=\frac{2Q}{MC}$$

Consider two energy input rates Q_1 and $Q_2 > Q_1$:

$$\left(\frac{dT_{Exit}(t)}{dt}\right)_1=\frac{Q_1\alpha}{mC_p}e^{-\alpha t},\quad \left(\frac{dT_{Exit}(t)}{dt}\right)_2=\frac{Q_2\alpha}{mC_p}e^{-\alpha t}$$

The ratio of the energy input rates Q_2/Q_1 at any time t is

$$\frac{Q_2}{Q_1}=\frac{\left(\frac{dT_{Exit}(t)}{dt}\right)_2}{\left(\frac{dT_{Exit}(t)}{dt}\right)_1}$$

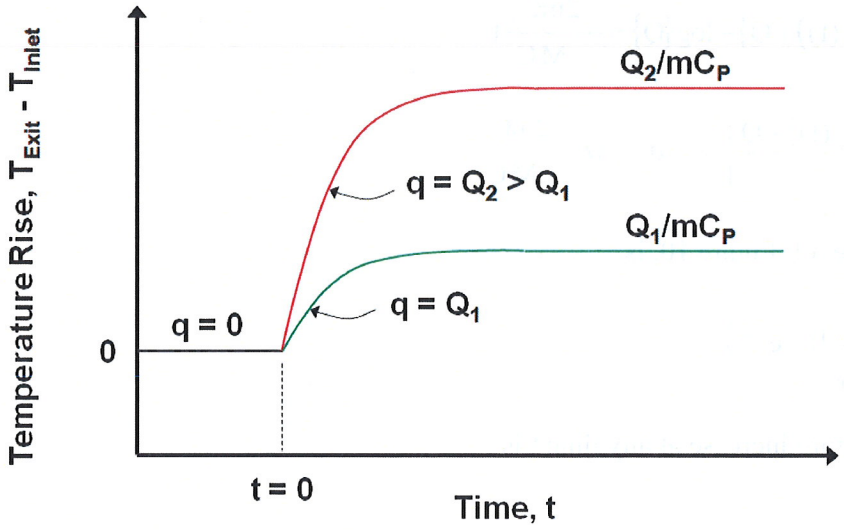

Figure 10. Coolant temperature rise vs. time

B. Calorimetry of Solid Fuel of the SF-CIHT Cell

In order to verify the results obtained in the SunCell experiment, a similar experiment was carried out in a calibrated calorimeter and the energy output was precisely measured. Using a 80mg, 2mm diameter silver shot with a small amount of partially hydrated doping and under an 95%Ar/5%H_2 atmosphere, the shot was ignited using a current of 20,000A. The energy released was observed to correspond to a total power of 141,000W. The results of a parallel optical power measurement (Absolute Power Spectrum of Ignited Hydrated Silver Shots, Table 1) also showed that under pure atmospheric pressure H2 gas the output power under similar conditions was negligible implying that pure molecular hydrogen gas is incapable of generating higher power densities. Atomic H is required in agreement with the hydrino reaction mechanism.

Table 1. Determination of the energy balance of the hydrino solid fuel by bomb calorimetry.

Experiment	Sample	Purpose	Purge	VI Energy Input (J)	VI Power Fitted Energy (J)	Room Temp @ Fire Time (°C)	Event Duration (End-Fire time) (min)	Total dT (°C)	Parr Calc'd dT (°C)	Pre Slope (°C/min)	Post Slope (°C/min)	Thermal Energy Out (J)	VI Power Fitted (J)	VI Power Fitted Gain (X)	VI Power Fitted Net (J)	VI Energy Input (J)	VI Energy Gain (X)	VI Net Energy (J)
2016-05-05-MY4	2016-05-05-MY4 75mg Empty Setaram Al Pan (Baked at 300C for 30 min), ~50 lbs., small cell #4, O-ring gasket, Std. Cu caps, Loaded in Argon GB, Tap 8, Heat 1, Preheated Tap 1 @ 10X	Testing disruptive waveform control	Ar GB, 5 min UHP Ar post load purge	253.3	199.1	22.67	5.25	0.0280	0.0354	-0.001932	-0.001180	226.6	199.1	1.14	27.5	253.3	0.89	-26.7
2016-05-05-MY3	2016-05-05-MY3 (1 mol%) pellet, 67.5mg, 175 lbs., small cell #4, O-ring gasket, Tap 8, Heat 1, Screw Tips	Testing batch 040816CC1 Ag+ (1mol%)	5 min 5% H2:Ar purge	386.1	252.1	22.29	6.18	0.0510	0.0585	-0.001931	-0.000984	374.1	252.1	1.48	122.1	386.1	0.97	-12.0
2016-05-05-MY2	2016-05-05-MY2 Ag+ [1 mol%) pellet, 75mg, 175 lbs., small cell #4, O-ring gasket, Tap 8, Heat 1, Screw Tips	Testing batch 040816CC1 Ag+ ¦1mol%) pellet	5 min 5% H2:Ar purge	370.6	231.3	21.72	7.58	0.0520	0.0581	-0.001663	-0.000609	371.8	231.3	1.61	140.5	370.6	1.00	1.2
2016-05-05-MY1	2016-05-05-MY1 Cu Caps control, 175 lbs., small cell, Heat 1, Screw Tips	Testing resistive control	5 min UHP Ar purge	261.3	261.3	21.38	4.95	0.0340	0.0392	-0.001741	-0.000797	250.6	261.3	0.96	-10.7	261.3	0.96	-10.7

Experimental:

The energy balances were measured on the HOH-based solid fuel samples each comprising an 80 mg silver shot having 1 mol% . The shots were formed by melting the silver and in a graphite crucible using an inductively coupled heater, rapidly quenching the molten mixture on an inert heat sink, and then punching the shot out of the solid slab. The shot comprised about 1 mole % water content. A tungsten foil heated in an argon-atmosphere glove box to dehydrate the hydrated surface coat served as the calibration control to determine the calorimeter heat capacity. An aluminum DSC pan (75 mg) (aluminum crucible 30 µl, D: 6.7 mm X 3 mm (Setaram, S08/HBB37408) and aluminum cover D: 6.7 mm, stamped, tight (Setaram, S08/HBB37409)) heated in an argon glove box for 30 minutes at 300 °C to remove hydrate was used as a control that melted and produced an arc plasma. The cell gas in all cases comprised argon-hydrogen (95/5%) at one atmosphere wherein the cell was purged for 5 minutes at a flow rate of 4800 sccm.

The setup of the Parr 1341 calorimeter used for the energy balance determination (Figure 1) comprised an unmodified calorimeter jacket (21) and calorimeter cover (1) (combined Parr part number A1100DD) [3]. A thermistor with a temperature resolution of 0.001°C (2) (Parr part number 1168E2) passed through the calorimeter cover and was secured such that it read the water temperature in line with the bomb assembly at a distance of 2.54 cm from the bottom of the water bucket (19). The custom made, 0.051 cm thick stainless steel oval bucket weighed 417.8 g and had a small diameter of 12.7 cm inches, a large diameter of 18.4 cm, and a height of 10.2 cm. The water bucket held 1225±.01 g of deionized water along with the custom calorimeter bomb assembly. A stirring assembly (6) comprised a stirrer pulley (Parr part number 37C2), a stirrer bearing assembly (Parr part number A27A), and stirrer shaft with impeller (11) (Parr part number A30A3). It was mounted on the calorimeter cover and was connected to the motor assembly (Parr part number A50MEB) by a motor pulley (8) (Parr part number 36M4) by a stirrer drive belt (7) (Parr part number 37M2) driven by the motor (9). The motor assembly was attached to the calorimeter externally by an L-bracket motor connector (10) to prevent the heat output of the motor from affecting the calorimetric measurements. Two 1.6 cm OD silver-plated, hollow copper electrodes (3) passed through customized holes in the calorimeter cover and further passed through a Teflon position stabilizing block and then connected to the main conductors of an ACME 75 kVA resistance welder. The 0.32 cm thick stainless steel custom cylindrical bomb cell (14) had a 7.62 cm diameter and 2.54 cm height with a 12.4 cm flange that was 0.64 cm thick. The electrodes penetrated the flange lid through electrode feed-throughs (13) with Teflon insulating ferrule seals (15) that provided electrical isolation and a hermetic seal.

Power was transmitted to the solid fuel (18) with or without the 1.3 cm diameter 0.48 cm thick copper fastener swivel (17) by the 3.0 cm long, 0.95 cm diameter copper sample-fastening bolts (16) which were threaded through the base of the electrodes. The solid fuel was contained between the fastener swivels by tightening the sample fastening bolts to a torque of approximately 1.81 Nm as measured by a high accuracy flat beam torque wrench resulting in approximately 1112 N force to the sample as measured by a piezoresistive force sensor (Measurement Specialties, FC2311-0000-0250-L). Efficient heat transfer was enabled by heat fins (12) installed on the electrodes immediately above the electrode feed-throughs that ensured minimal heat loss through the electrodes and out of the closed system. The bucket stand (20) elevated the bomb cell to the top of the calorimeter to minimize the dimensions and quantities of materials necessary to operate the Parr 1341 calorimeter and improve the accuracy of the measurements.

Each sample was ignited with an applied peak 60 Hz voltage of less than 10 V and a peak current of about 20,000 A. The input power was recorded through a custom interface receiving input from the positive probe connector (4) and negative probe connector (5). The input energy of the calibration and ignition of the solid fuel was given as the product of the voltage and current integrated over the time of the input. The voltage was measured by a data acquisition system (DAS) comprising a PC with a National Instruments USB-6210 data acquisition module and Labview VI. The current was also measured by the same DAS using a Rogowski coil (Model LFR15/150/700) that was accurate to $\pm 0.3\%$ as the signal source. V and I input data were obtained at 83 KS/s and a voltage attenuator was used to bring analog input voltage to within the +/-10V range of the USB-6210.

The input power data was processed to calculate the input energy during the rapid power decay following ignition to an open circuit. Taking the product of the measured voltage waveform obtained from the voltage taps immediately above the water level on the 5/8" OD Cu rods and the measured current waveform given by the Rogowski coil yielded the power waveform. The time integrated power waveform yielded the cumulative energy provided to the system to the time point that the ignition or detonation event occurred. The secondary circuit of the spot welder transformer was temporarily broken as the electrode tips were pushed apart by the force of the blast. On a time scale of about 10 μs, the circuit quickly transitioned to high resistance, effectively becoming an open circuit with the development of a reactive voltage transient as a result of the fast collapsing magnetic flux in the transformer. The current fell to zero as the voltage transient produced a corresponding reflected wave reactive power component in the power waveform that typically rapidly decayed on the order of about 500 μs to 1 ms. To eliminate this reactive power component over the time of the current decay, the power waveform was smoothed over the immediate post-blast period until current reached zero by fitting the

voltage and current components during this time to their typical amplitudes and phases during pre-blast conditions. The accuracy of this method was confirmed by the achievement of energy balance with control samples.

Figure 1. The setup of the Parr 1341 calorimeter used for the energy balance determination.

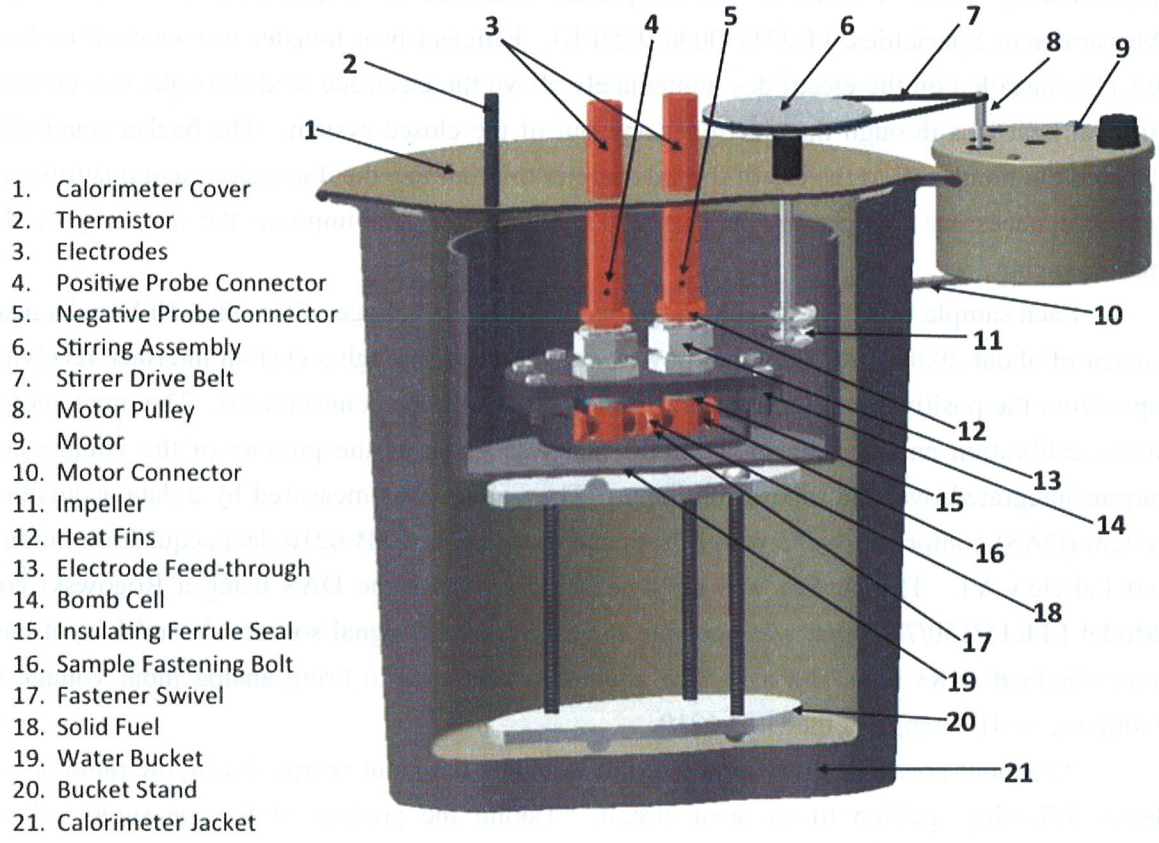

III. Results and Discussion

Using the W metal foil in Table 1, the heat capacity of the calorimeter and electrode apparatus used to measure the energy balance of solid fuel samples was determined to be 6400 J/°C. The calorimetry method used to determine the thermal output from the temperature versus time response following equilibration and ignition was the analytical method described in the operating manual of the Parr 1341 bomb calorimeter [6]. The net energy is the difference between the thermal output and energy input.

As shown in Table 1, near zero net energy balance was measured on the control Al DSC pan which was conditioned to remove as much H and O as possible. In contrast, significant energy and power was observed for the HOH-based solid fuel wherein HOH served as catalyst.

Up to 141 J was recorded for a 1 ms ignition event corresponding to an average power of 141,000 W. The power from other methodologies such as absolute spectroscopy on the ignition of hydrated silver shot and the coolant thermal response with the addition of an to an injected molten silver stream exposed to argon-H_2 (95-5%) flow was higher due to the larger reaction volumes compared to the limited-volume calorimetric cell. Moreover, the net energy could be higher than reported considering that a significant portion of the input energy was dissipated in the two joints and the bus bars of the calorimeter fuel ignition circuit with only about 50% of the input energy actually delivered to the fuel sample to cause it to ignite. For , no theoretical energy exits since the no exothermic reaction was possible between argon, hydrogen, , and silver.

References

1. R. Mills, *The Grand Unified Theory of Classical Physics*; 2014 Edition, posted at http://www.blacklightpower.com/theory-2/book/book-download/.
2. R. Mills, J. Lotoski, W. Good, J. He, "Solid Fuels that Form HOH Catalyst," Int'l J. Hydrogen Energy, 39 (2014), pp. 11930–11944 DOI: 10.1016/j.ijhydene.2014.05.170.
3. R. Mills J. Lotoski, "H_2O-based solid fuel power source based on the catalysis of H by HOH catalyst", Int'l J. Hydrogen Energy, Vol. 40, (2015), 25-37.
4. R. Mills, X Yu, Y. Lu, G Chu, J. He, J. Lotoski, "Catalyst induced hydrino transition (CIHT) electrochemical cell," (2012), Int. J. Energy Res., (2013), DOI: 10.1002/er.3142.
5. R. Mills, J. Lotoski, J. Kong, G. Chu, J. He, J. Trevey, "High-Power-Density Catalyst Induced Hydrino Transition (CIHT) Electrochemical Cell." Int. J. Hydrogen Energy, 39 (2014), pp. 14512–14530 DOI: 10.1016/j.ijhydene.2014.06.153.
6. http://www.parrinst.com/products/oxygen-bomb-calorimeters/1341-plain-jacket-bomb-calorimeter/.

C. Power Determination of the Light Emanating from Ultra-low field ignition of Hydrated Silver Shots:

One of the spectacular features of this experiment is the nature of the light that is released by the ignition of hydrated silver shots under low-voltage and high-current. It is quite intriguing that the majority of the light emitted lies in the 10-300 nm regions, with very little if any in the higher wavelengths. Clearly, this is a very important result and warrants a comprehensive debate in the scientific community. The peak power in the 22.8-647 nm spectrum was an astonishingly high value of 2.1 MW corresponding to 84J in 40us. In several experiments, for a total ignition input power of 25 kW, the emitted light had an optical power of 950 kW. When the experiments were carried out either in anhydrous shots or pure molecular hydrogen

the power outputs were significantly low. The following summarizes the experimental conditions and other pertinent details.

Experimental Method: Absolute Power Spectrum of Ignited Hydrated Silver Shots

Schematics of the light source comprising hydrated silver shot ignited with a spot welder, the intensity reducing, evacuated light conduit, and each of the spectrometers, ultraviolet-visible, normal incidence, and grazing incidence to cover the wavelength range 815-10 nm are shown in Figures 1A, 1B, and 1C, respectively. Silver shots of about 1.24 mm radius, weighing about 80-90 mg were formed by dripping molten silver through a 0.1 mm diameter dripper into distilled water maintained at room temperature. The shots were retrieved and agitated to remove excess water, but were not dried. The water content was determined by weighing about 10 g, before and after melting in the glove box to remove the water content which as determined to be about 1 mol%. The shots were singly fired in a vacuum chamber (14.6 cm diameter X 28 cm length) with a windowless connection to the vacuum tube (3.5 cm ID) that was either connected to the GIS, the NIS (EUV wavelengths), or a MgF_2 window (7 mm diameter, 2 mm thickness) that was incident to the entrance optics of the NIS (UV-Vis wavelengths) or the Mightex spectrometer. The chamber and tube were evacuated to 1 X 10^{-3} Torr (NIS and UV-Vis) or 5 X 10^{-4} Torr (GIS) as different spectral regions were acquired. When the MgF_2 window was absent, the EUV spectrometers were differential pumped to 1 X 10^{-6} Torr in order to record the EUV wavelengths. Each shot was confined between the two copper electrodes of a spot welder (Taylor-Winfield model ND-24-75 spot welder, 75 KVA, 15 PSI applied electrode pressure) wherein the electrodes penetrated the vacuum chamber at vacuum-sealed, electrically insulating penetrations. The horizontal plane of the sample was aligned with the optics of each spectrometer as confirmed by an alignment laser. Each sample was subjected to a short burst of low voltage, high current electrical energy. The applied 60 Hz AC voltage was less than 1 V across the shot, and the peak current was about 23,000-25,000 A at an applied total voltage of about 6 V. The high current caused the sample to ignite as brilliant light-emitting expanding plasma of near atmospheric pressure. To cause the plasma to become optically thin such that EUV light could emerge, the ignition occurred in the 4.7 liter vacuum chamber that housed the ignited sample.

The EUV spectrum (5-65 nm) was recorded using a McPherson grazing incidence EUV spectrometer (Model 248/310G) equipped with a 600 g/mm gold coated grating. The angle of incidence was 87°. The wavelength resolution with an entrance slit width of 200 □m was about 0.3 nm at the CCD center and 0.7 nm at the limits of the CCD wavelength range window of 50 nm. A 150 nm thick aluminum filter (Luxel Corporation) was placed between the grating and

CCD detector to block the visible light and to prevent damage to the spectrometer from the blast debris. The Al filter has a transmission window between 17 nm to 80 nm as shown in Figure 2A. To measure to the 10.1 nm short wavelength cutoff, a 150 nm thick Zr filter (Luxel Corporation) was placed in the light path between the grating and CCD detector. The transmittance of the Zr filter has a transmission window in the region of 10 nm as shown in Figure 2B. The evacuated distance from the shot to the slits was 1.48 m. The EUV light was detected by a CCD detector (Andor iDus) cooled to -60 °C. The CCD detector was centered at 25 nm and 55 nm to cover the wavelength region of 0-65 nm.. Known oxygen and lines observed in a high voltage pulse discharge spectrum were used to calibrate the wavelengths of the 0 to 65 nm region prior to recording the shot blast spectrum.

The shot light emission was introduced to a normal incident EUV spectrometer for spectral measurement of the wavelength region covered by the monochromator of 30-650 nm. The spectrometer was a McPherson 0.2 meter monochromator (Model 302, Seya-Namioka type) equipped with a 300 g/mm Al-MgF_2 coated grating. The EUV light was detected by the Andor iDus CCD camera. The slits were set at ~10 μm. The vacuum inside the monochromator was maintained below 1 X 10^{-6} Torr by a turbo pump. The evacuated distance from the shot to the slits was 1.20 m. The calibration of the spectral intensity was obtained by matching the intensity in regions of wavelength overlap (210.8 to 647 nm) with the spectrum of a UV-Vis spectrometer that was calibrated with a NIST traceable quartz tungsten halogen lamp and a deuterium/W lamp.

The shot light emission was introduced to a UV-Vis Mightex system spectrometer for spectral measurement of the wavelength region 200-815.4 nm that was calibrated with NIST traceable W and deuterium/W lamp lamps. The Mightex system is comprised (i) a Horiba MicroHR f/3.9 imaging spectrometer (Model: MHR-MS) with variable entrance slit of from 10 um to 2 mm width by 1 mm or 3 mm high, a single grating mount (Model: MHR-SGM), and a 150 g/mm ruled grating blazed at 500 nm (Model: 510-49-X36), (ii) a Mightex buffered and triggerable USB 2.0 CCD linescan camera (Model: TCE-1024-UF) with 1024 pixels of 14 x 14 um size per pixel, spectral range from 200 to 1000 nm, 8 bit ADC at 25 kFPS, and 40 us minimum exposure time, and (iii) a MgF_2 window (7 mm diameter, 2 mm thickness) on the entrance to the spectrometer and a fused silica window on the entrance of the camera. The Mightex was triggered by a 30 us duration 5V signal generated by an Agilent 33220A 20 MHz Arbitrary Waveform Generator when a gating signal generated by a Picoscope 5442B digital oscilloscope was issued when current began to flow above a threshold in the welder as measured by a Rogowski current probe (Model: PEM LFR15/150/700).

The parameters during acquisition and data processing of the GIS-NIS-Mightex acquisition sequence as used by the Mightex were: the Horiba spectrometer center was 500 nm,

the slit width was 30 um, the slit height was 1 mm, the exposure time was 40 us, the frame rate was 25,000 frames/s (FPS) wherein 2000 frames were acquired over an 80 ms acquisition time, the evacuated path distance from the silver shot to the MgF_2 window was 1.15 m, the light exited the window to travel 0.05 m in air to the Mightex slits such that the total distance from the shot to the slits was 1.20 m, and the absolute irradiance integration range was 200-815.4 nm. The spectra were wavelength calibrated using emission lines generated by a mercury argon wavelength calibration source (Model: Ocean Optics HG-1). A 3rd order polynomial was used to generate the pixel to wavelength mapping. The absolute intensity calibration was performed using a Newport Calibrated Source Lamp, Quartz Tungsten Halogen (QTH), 1000 W, confirmed calibration to NIST traceable standards over 250-2400 nm, (Model: 63350). The QTH calibration lamp setup was described previously [7]. The instrument response function of the Mightex absolute irradiance calibration using the QTH lamp was extended to 200 nm using a Hamamatsu L10290 D2/W combo source with known relative irradiance by direct coupling to the Mightex. The relative irradiance of the Hamamatsu source was matched to the absolute irradiance in the region of 350 nm as calibrated by the QTH lamp to determine the UV region instrument response function.

The 5 nm to 65 nm region was recorded with the GIS. The CCD dark counts were subtracted from all spectra. The spectrum recorded with the CCD centered at 25 nm using the Zr filter (Figure 2B) was corrected by dividing the data by the wavelength-matched Zr filter curve. The spectrum recorded with the CCD centered 55 nm using the Al filter was corrected by dividing the data by the Al filter curve (Figure 2A). Matching the intensities at overlapping spectral wavelengths was used to join the 25 nm and 55 nm curves. The joined spectrum was corrected for the efficiency of the Au coated grating by dividing the data by the grating efficiency curve (Figure 3). The wavelength calibration was achieved using the spectrum from a high voltage discharge in air (Figure 4).

The 25 nm to 650 nm region was recorded with the NIS. The CCD dark counts were subtracted from all spectra. Spectra were recorded with the CCD centered at 100, 200, 300, 400, and 500 nm using the MgF_2 window except in the case of the 100 nm and 200 nm spectra since those wavelengths were cutoff by the window. The 300, 400, and 500 nm spectra were corrected for the attenuation by the MgF_2 window by using the curve that matched the 100 nm and 200 nm spectra with the window to those without. The efficiency of the window is given in Figure 5. Matching the intensities at overlapping spectral wavelengths was used to join the curves. The joined spectrum was corrected for the reflectance but not the efficiency of the NIS 300G Al-MgF_2 coated grating by dividing the data by the grating reflectance curve (Figure 6) only. The spectrum was not corrected for the grating efficiency curve shown in Figure 6 since it was a theoretical curve provided by the vendor McPherson and was not well known to short

wavelengths where the most significant correction exists. Work is in progress to use the SunCell® blackbody curve in the deep UV to calibrate the grating efficiency.

Matching the intensities at overlapping spectral wavelengths was used to join the corrected curves of the GIS and the NIS. The joined spectrum was corrected for the efficiency of the CCD by dividing the data by the wavelength-matched CCD quantum efficiency curve (Figure 7). The spectral count intensity was converted to energy density by multiplying the counts as a function of wavelength by the conversion factor $\frac{hc}{\lambda}$.

The 200 nm to 815 nm region was recorded with the Mightex UV-Vis spectrometer using the MgF_2 window. The spectrum was corrected by dividing the data by the transmission efficiency of the window (Figure 5). The UV-Vis spectral results were used to scale the GIS-NIS combined spectrum to achieve a match in the spectral overlap region. The integrated power of the Mightex spectrum was determined over the wavelength region 210.8-647 nm. The GIS-NIS spectrum was scaled such that the integrate power in the 210.8-647 nm region matched that of the Mightex spectrum. The total power over the full wavelength range of 22.8-647 nm was integrated on the combined spectrum.

Using the Mightex UV-Vis spectrometer, absolute spectroscopy was also recorded over the wavelength range of 200-815 nm on ignited partially hydrated 80-90 mg silver- (3-6 mole %) and silver- (6 mole %) shots wherein served as a source of by thermal decomposition. The salt-containing shots were formed by mixing the salt into molten silver in a graphite crucible maintained at 1100 °C in the glove box by an inductively coupled heater. The melt was rapidly quenched on a stainless steel metal block, and shots were produced with a metal punch. Using the spot welder, the shots were ignited in the chamber having the windowless connected vacuum-capable tube with the MgF_2 window at the far end from which light entered the Mightex spectrometer. The shots were run under vacuum and 1 atm pure H_2. The power of the spot welder was recorded as a function of time at a time resolution of 56 or 104 ns via 60 MHz digital oscilloscope (Picotech, Picoscope 5442B) using a voltage and current probe. The voltage was measured by a 25 MHz 70V 10:1 differential voltage probe (Picotech, model TA041) accurate to +/-2% and the current was measured with a Rogowski coil (PEM, LFR 15/150/700) that was accurate to +/-0.3%. The light power was recorded as a function of time with the Mightex on a 40 μs time scale and compared to the ignition power at the same time point of maximum power emission.

III. Results and Discussion

The hydrated silver shots comprising a source of H atoms were ignited by passing a low voltage, high current through the shot to produce explosive plasma that emitted brilliant light predominantly in the short-wavelength (10 to 300 nm) region. The GIS was corrected for the Al and Zr filter curves shown in Figure 2A-B as well as for the grating efficiency (Figure 3). The NIS data was corrected by the MgF_2 window attenuation using data with and without the widow. The NIS spectrum was further corrected by the reflectance curve but not the efficiency curve of the Al-MgF_2 coated 300 g/mm grating shown in Figure 6. The UV-Vis spectrum was corrected for the MgF_2 window transmission curve shown in Figure 5 and was absolutely calibrated. The raw spectra obtained using the GIS and NIS is shown in Figure 8. The combined GIS and NIS spectra following filter, grating, and CCD quantum efficiency corrections is shown in Figure 9. Figure 10 shows the combined GIS and NIS spectra before power calibration against the absolutely calibrated UV-Vis spectrum wherein the spectral count intensity of Figure 9 was converted to energy density by multiplying the counts as a function of wavelength by the conversion factor $\frac{hc}{\square}$.

The Mightex UV-Vis (200-815.4 nm) spectrum was corrected by dividing the data by the transmission efficiency of the window (Figure 5). The UV-Vis spectral results used to scale the GIS-NIS combined spectrum to achieve a match in the spectral overlap region were a peak emission power (40 us resolution) of 424.8 kW, a total emission energy of 96.4 J, a total emission time of 0.76 ms, and a time averaged emission power of 126.9 kW. The integrated power of the Mightex spectrum was determined over the wavelength region 210.8-647 nm. The GIS-NIS spectrum was scaled such that the integrate power in the 210.8-647 nm region matched that of the Mightex spectrum. The total power over the full wavelength range of 22.8-647 nm was integrated on the combined spectrum. The full wavelength calibrated and absolute intensity calibrated emission spectrum (22.8-647 nm) is shown in Figure 11. The peak and average powers of the light released from the shot ignition event determined using absolute spectroscopy over the 22.8-647 nm region were 2.1 MW and 514,000 W corresponding to 84 J in 40 us and 391 J in a 0.76 ms blast event, respectively.

In addition to the transmission and efficiency of the optical collection and recording components of the spectroscopy systems, a number of other factors have been considered in the power determination. The power from arc plasma driven by an axial electric field can be emitted in a dipole distribution that results in a $\cos^2\square$ power distribution and a 1/4 total power correction from that measured at the peak intensity. However, as evidenced by high speed photography, the nature of the emission in the case of the shot ignition is an explosion with a spherical wave that propagates out in all directions uniformly except where it is blocked by a physical object such as the electrodes where the power is absorbed to result in recoil of the welder arms and electrodes

Figure 12. The wavelength calibrated and absolute intensity calibrated spectrum (10-480 nm) of the emission of hydrated silver shots taken with a new grating. The radiation is predominantly in the high-energy region with the predicted short wavelength emission of the H(1/4) continuum radiation and the short-wavelength H(1/4) cutoff is observed at 10.1 nm.

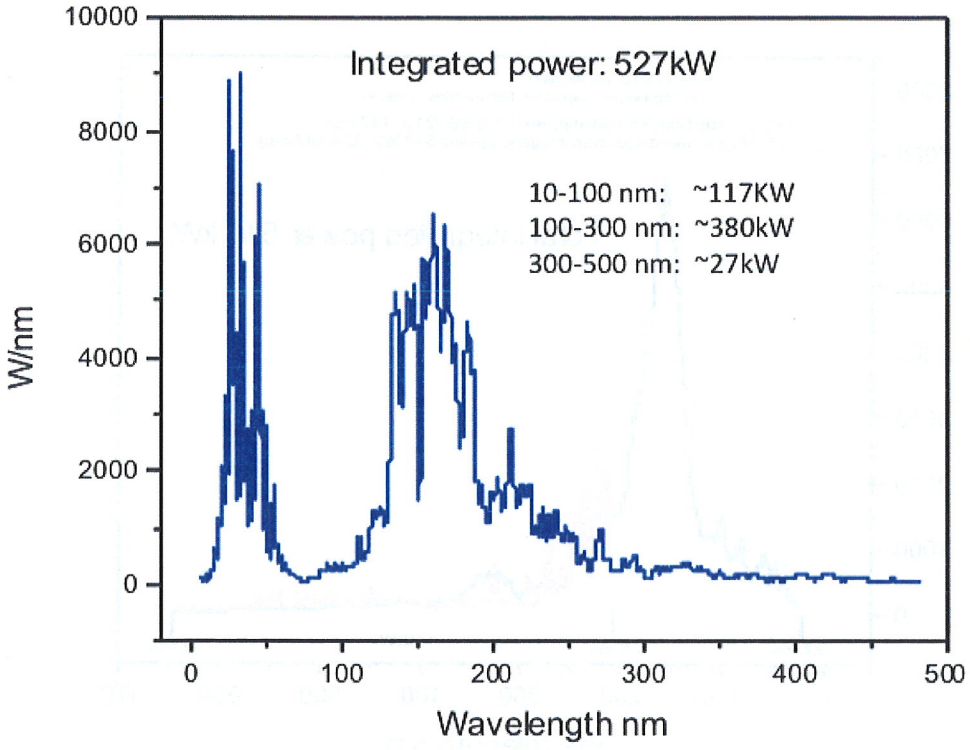

and molten silver coating, evulsion, and melting of the copper electrodes. The optical power determination was under determined by a plurality of mechanisms. The NIS spectrum was only corrected for the 300G Al-MgF_2 coated grating reflectance (Figure 6, upper trace) and not the efficiency as well (Figure 6, lower trace). The efficiency was only known theoretically as provided by McPherson and was not well known especially at short wavelengths wherein significant corrections and resulting increases in intensity are expected. Further reducing the spectral intensity, the grating had lost some efficiency in the short wavelength region due to Ag coating it. This can be appreciated by comparing the short wavelength region spectrum shown in Figure 11 with a spectrum taken at an earlier time when the grating had less exposure to Ag blast debris (Figure 12). There are three additional factors that were not quantified that diminish the reported power below that actually emitted by the shot blast event: (i) The solid angle for light collection by the spectrometers is greatly reduced by electrode shadowing. It was found that if the electrodes were not beveled, essentially no light gets out. (ii) A related issue with the use of the 1.6 cm diameter electrodes, the great separation distance, and very narrow slits is that the electrodes block the light by reducing the solid angle such that sample-spectrometer alignment is critical. It was very likely that the light was recorded off angle from the sample plane at a diminished light intensity due to electrode shadowing since it is very difficult to perfectly align on axis especially given the movement with the blast event. (iii) The blast vapor and debris are optically thick until the plasma expands to become thinner. If fact, no EUV light was initially observed until a vacuum chamber was used to allow the plasma to expand to become thin enough for the EUV transparency. A substantial amount of the EUV light is absorbed when the power is the greatest in the first time increment following the blast and before transparency is achieved.

It was remarkable that the radiation was essentially all short wavelength in the EUV and UV range with essentially no visible or near infrared light (Figure 11). The power density was high considering the source of the more than 514,000 W was produced by a shot of less than 10 microliter volume. This result is even more extraordinary considering the peak power was 2.1 MW.

To search for the 10.1 nm short wavelength cutoff while selectively blocking visible light, a 150 nm thick Zr filter (Luxel Corporation) that has a transmission window in the region of 10 nm (Figure 2B) was placed in the light path between the grating and CCD detector. The emission spectrum of the hydrated Ag shot plasma emission using a grating that was not degraded in the short wavelengths showed strong EUV continuum having a 10.1 nm cutoff as predicted [1-4] as shown in Figure 12.

The results of the absolute spectroscopy (200-815.4 nm) recorded on ignited partially hydrated 80-90 mg silver- (3-6 mole %) and silver- (6 mole %) shots wherein served as a source of by thermal decomposition are given in Table 1. The peak

power of silver- (3-6 mole %) and silver- (6 mole %) shots of about 950,000 W (40 us time resolution) was higher than the non-reactive ignition power of 25,000 W (104 us time resolution). The total optical power of the 22.8-647 nm region was shown to be about 4.1 times the optical power in the UV (>200 nm) range; so the total peak optical power is much higher, greater than 3.9 MW. It was found that a pure H_2 atmosphere that favored molecular hydrogen and suppressed the atomic H hydrino reactant essentially eliminated the optical power.

References

1. R. L. Mills, Y. Lu, "Hydrino continuum transitions with cutoffs at 22.8 nm and 10.1 nm," Int. J. Hydrogen Energy, 35 (2010), pp. 8446-8456, doi: 10.1016/j.ijhydene.2010.05.098.
2. R. L. Mills, Y. Lu, K. Akhtar, "Spectroscopic observation of helium-ion- and hydrogen-catalyzed hydrino transitions," Cent. Eur. J. Phys., 8 (2010), pp. 318-339, doi: 10.2478/s11534-009-0106-9.
3. R. L. Mills, Y. Lu, "Time-resolved hydrino continuum transitions with cutoffs at 22.8 nm and 10.1 nm," Eur. Phys. J. D, Vol. 64, (2011), pp. 65, DOI: 10.1140/epjd/e2011-20246-5.
4. R. L. Mills, R. Booker, Y. Lu, "Soft X-ray Continuum Radiation from Low-Energy Pinch Discharges of Hydrogen," J. Plasma Physics, Vol. 79, (2013), pp 489-507; doi: 10.1017/S0022377812001109.
5. A. Bykanov, "Validation of the observation of soft X-ray continuum radiation from low energy pinch discharges in the presence of molecular hydrogen," http://www.blacklightpower.com/wp-content/uploads/pdf/GEN3_Harvard.pdf.
6. R. Mills, J. Lotoski, Y. Lu, "Mechanism of soft X-ray continuum radiation from low-energy pinch discharges of hydrogen and ultra-low field ignition of solid fuels", (2016), submitted, http://brilliantlightpower.com/wp-content/uploads/papers/Cont_EUV_HOH-031215.pdf.
7. Newport Light Sources document, Figure 2 (page 16: http://assets.newport.com/webdocuments-en/images/light_sources.pdf).

Table 1. The results of the absolute spectroscopy recorded on ignited hydrated silver shots, at least partially dehydrated silver shots, and partially hydrated 80-90 mg silver- (3-6 mole %) and silver- (6 mole %) shots over the wavelength range of 200-815.4 nm.

Setup Atm	Sample Type	Sample Mass (mg)	Peak Waveform Current (kA)	Mightex Energy (J)	Max Power (kW)
Vacuum	Ag+ (6mol%)-RF050616	66.7	17.9	107.5	306.6
Vacuum	Ag+ (6mol%)-RF050616	82.1	20.5	94.7	309.7
Vacuum	Ag+ (6mol%)-RF050616	87.7	19.1	202.8	735.6
Vacuum	Ag+ (6mol%)-RF050616	82.0	18.5	150.3	543.8
Vacuum	Ag+ (3mol%)-CC050416	76.6	22.1	256.6	945.9
Vacuum	Ag+ (3mol%)-CC050416	67.0	20.2	49.2	194.4
Vacuum	Ag+ (3mol%)-CC050416	78.4	23.6	60.9	238.8
H2	Ag+ (3mol%)-CC050416	64.0	11.7	2.5	34.2
H2	Ag+ (3mol%)-CC050416	72.3	11.2	13.9	113.2
H2	Ag+ (3mol%)-CC050416	62.0	22.1	7.0	67.0
H2	Ag+ (3mol%)-CC050416	72.3	24.3	1.6	2.9

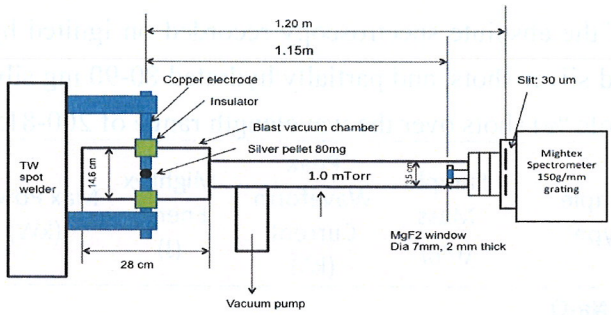

(A)

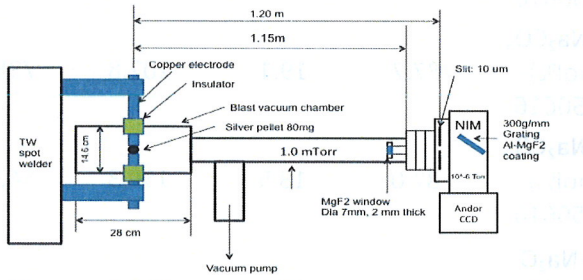

(B)

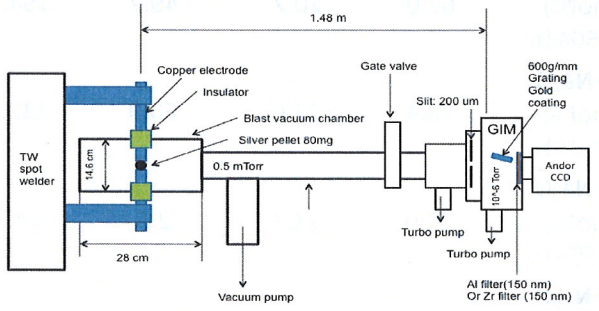

(C)

Figures 1A-C. Schematics of the light source comprising hydrated silver shot ignited with a spot welder, the intensity reducing, evacuated light conduit, and each of the three spectrometers to cover the spectral wavelength range of 10 nm to 815 nm. (A) Grazing incidence EUV spectrometer (GIS). (B) Normal incidence EUV spectrometer (NIS). (C) Ultraviolet-visible (UV-Vis) spectrometer.

(C)

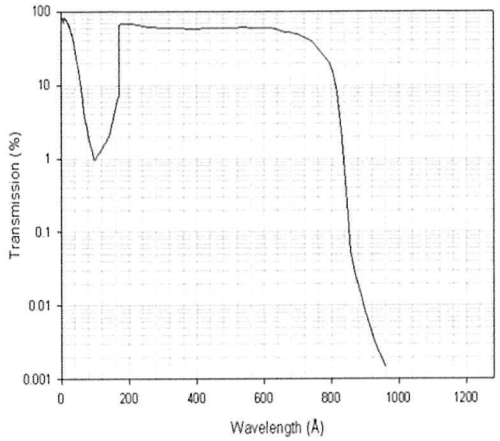
100
10
1
0.1
0.01
0.001
Transmission (%)
0
200
400
600
800
1000
1200
Wavelength (Å)

(A)

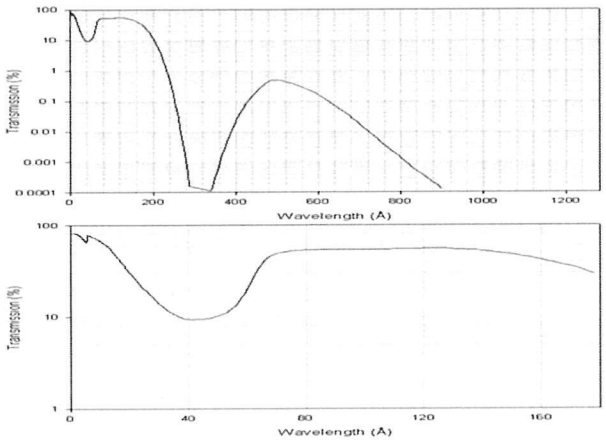
100
10
1
0.1
0.01
0.001
0.0001
Transmission (%)
0
200
400
600
800
1000
1200
Wavelength (Å)
100
10
1
Transmission (%)
0
40
80
120
160
Wavelength (Å)

(B)

Figures 2A-B. Transmission curves of filters for EUV light that blocked visible light. (A) The Al filter (150 nm thickness) having a cutoff to short wavelengths at ~17 nm. (B) The Zr filter (150 nm thickness) having high transmission at the predicted H(1/4) transition cutoff 10.1 nm.

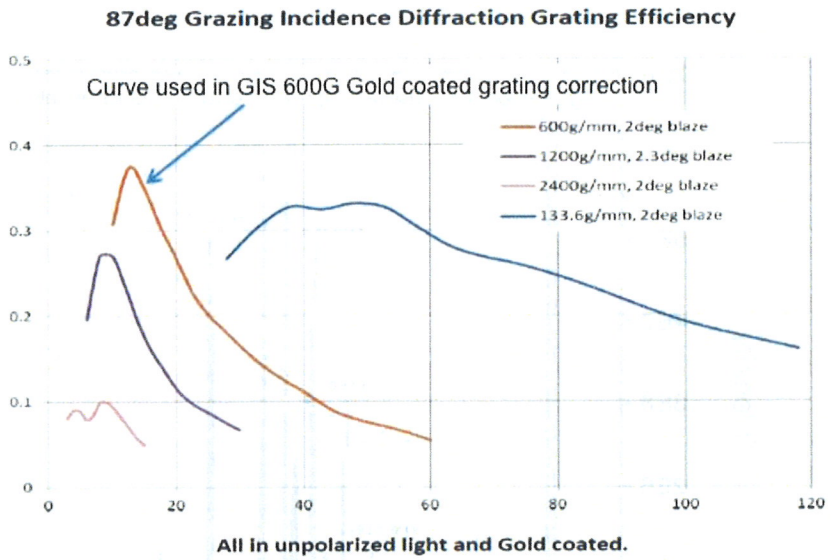

Figure 3. The efficiency of the Au 600 g/mm grating that was used to correct the GIS raw spectrum

Figure 4. The EUV spectrum (5-50 nm) recorded with the GIS on a high voltage discharge of air that was used for wavelength calibration using the positions of known oxygen and ions.

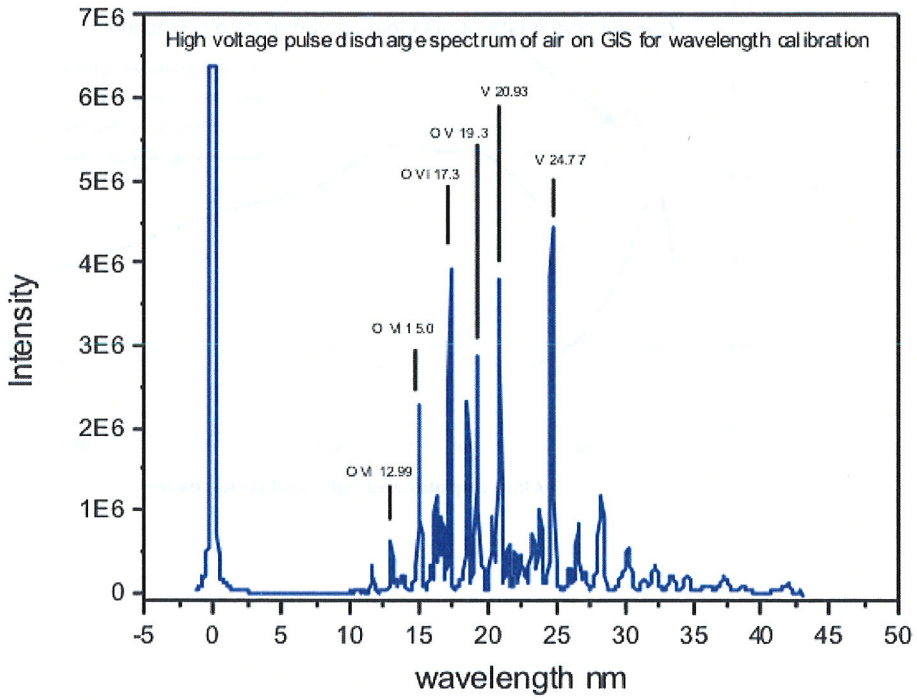

Figure 5. Transmission curve of the MgF_2 window that was used to correct the raw spectra acquired with the window.

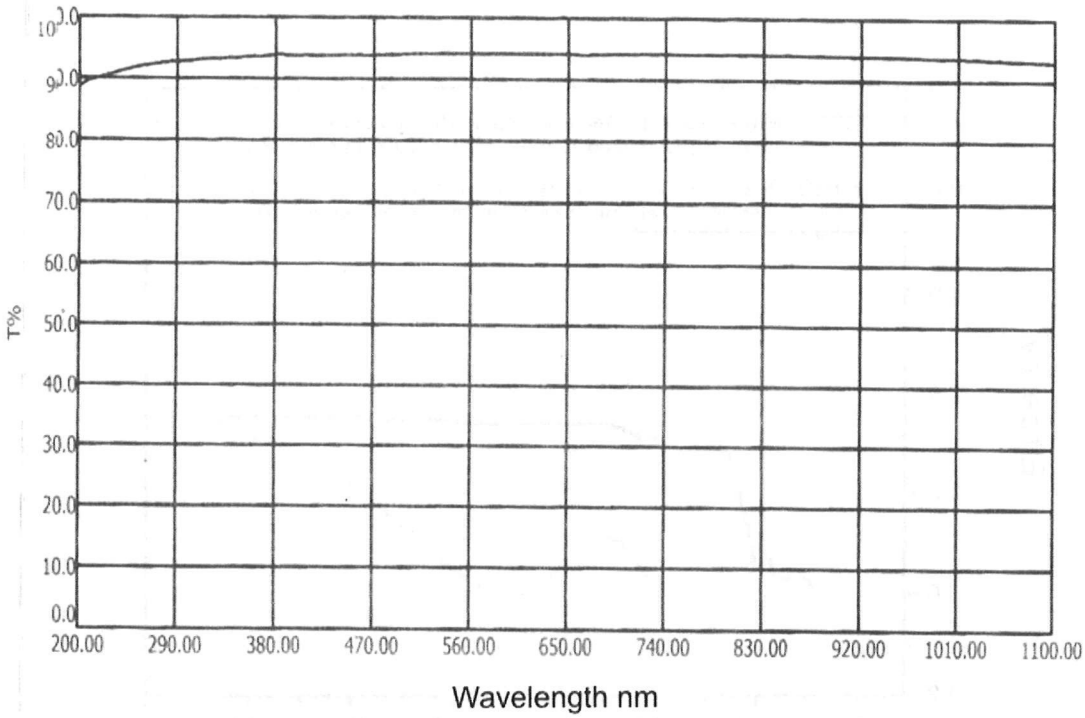

Figure 6. The reflectance and the efficiency of the Al-MgF_2 coated 300 g/mm grating. The NIS spectrum was only corrected by the reflectance since the efficiency was not well characterized.

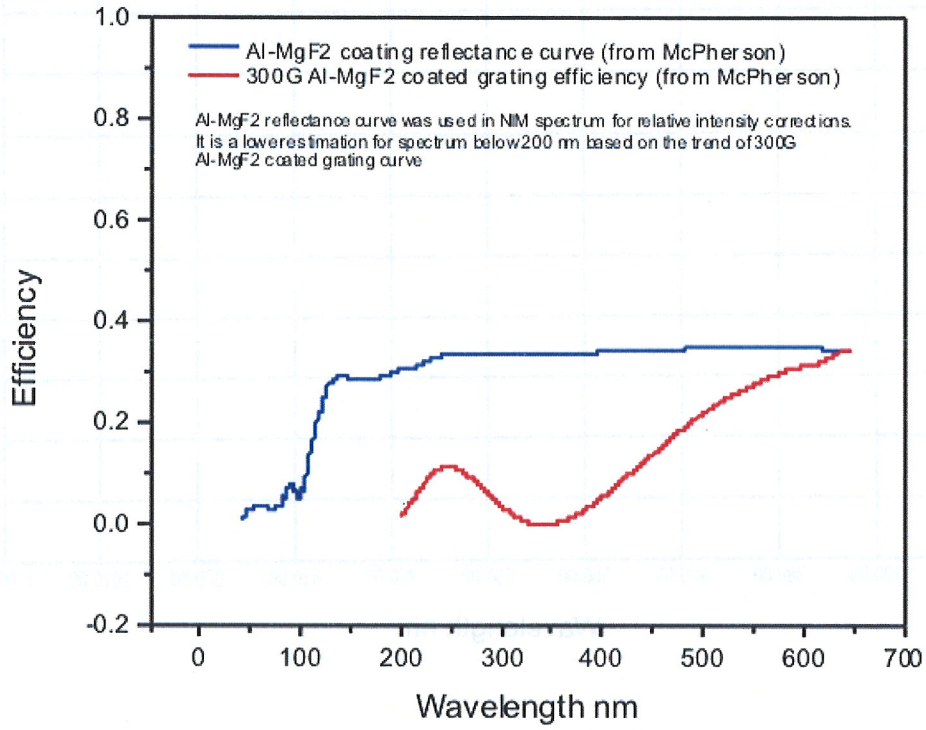

Figure 7. The CCD quantum efficiency that was used to correct the GIS and NIS raw spectra.

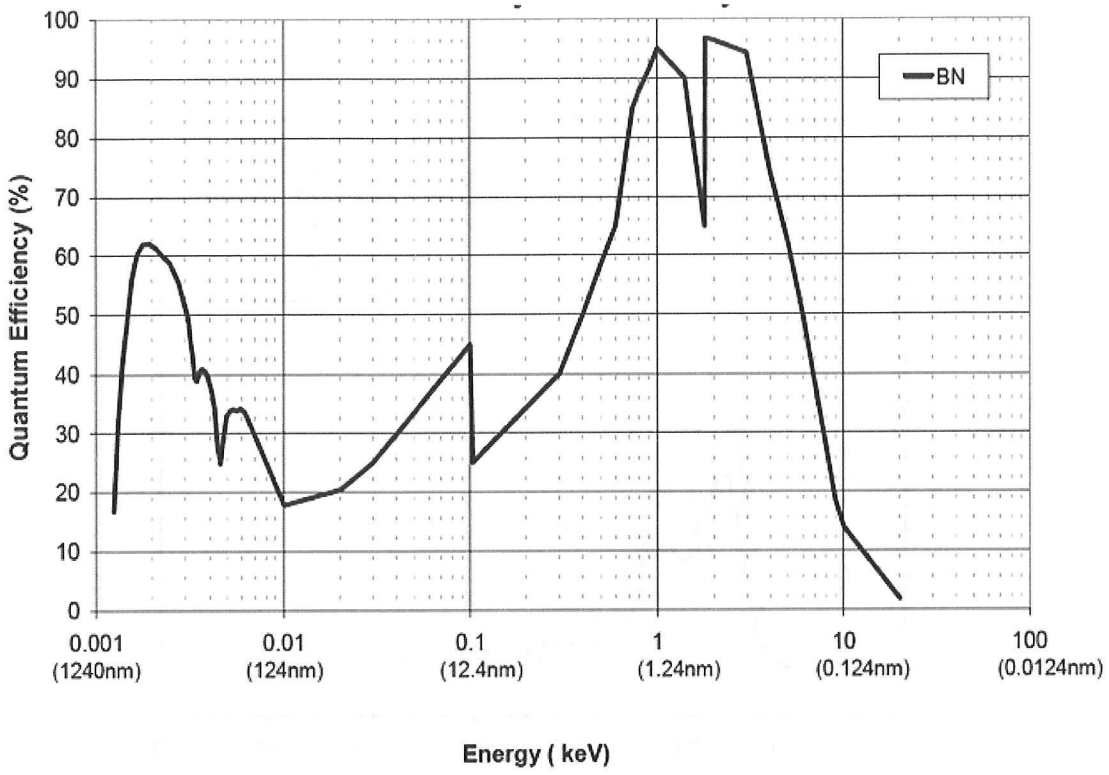

Figure 8. The raw spectra obtained using the GIS and NIS spectrometer to be processed with window, filter, grating, and CCD quantum efficiency corrections.

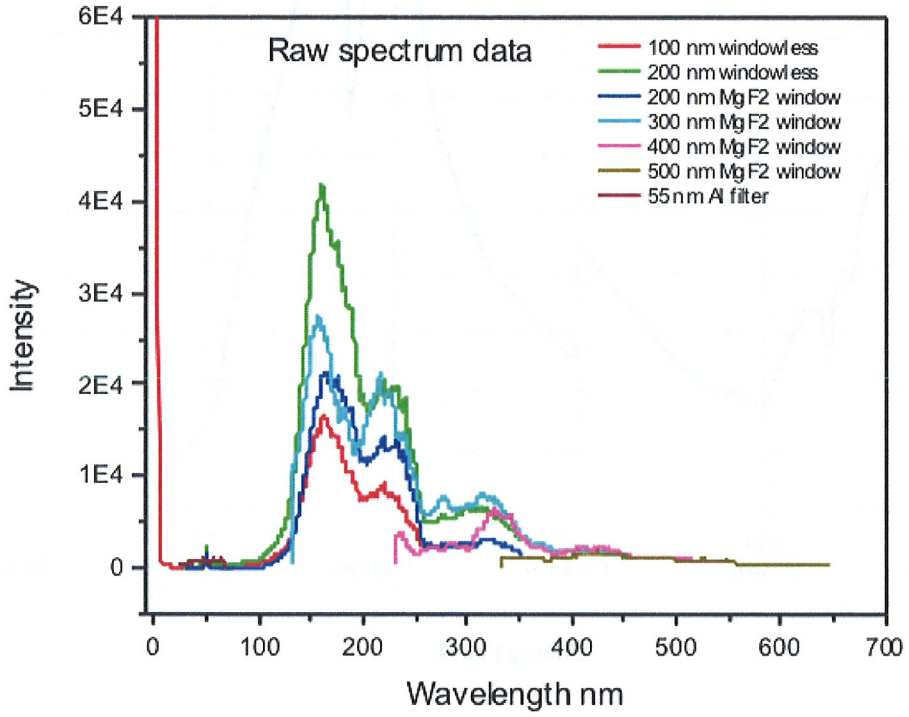

Figure 9. The combined GIS and NIS spectra following filter, grating, and CCD quantum efficiency corrections.

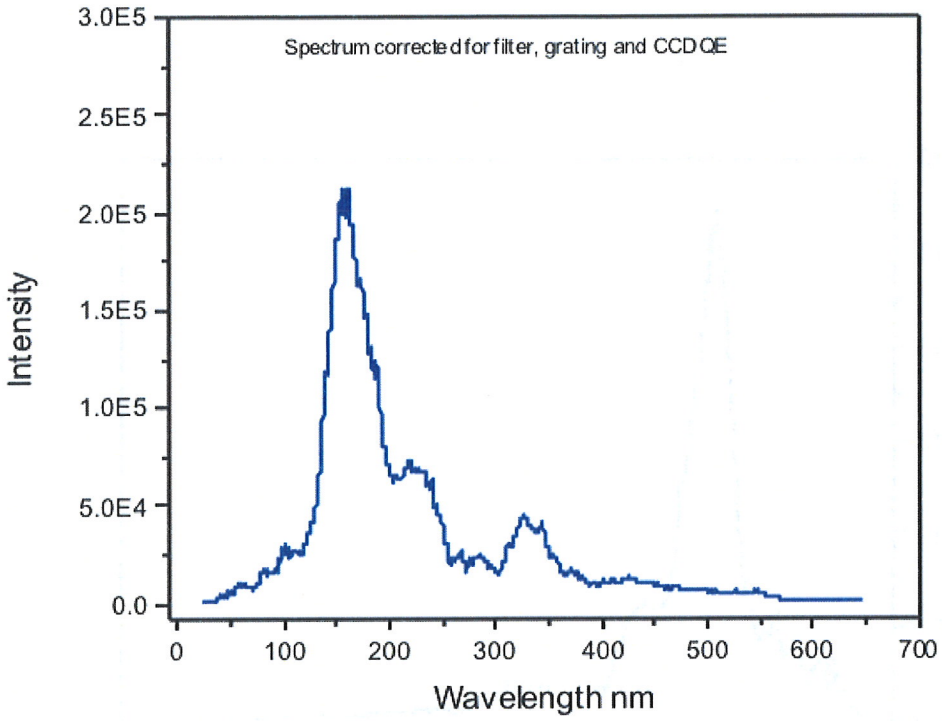

Figure 10. The combined GIS and NIS spectra before power calibration against the absolutely calibrated UV-Vis spectrum wherein the spectral count intensity of Figure 9 was converted to energy density by multiplying the counts as a function of wavelength by the conversion factor $\frac{hc}{\square}$.

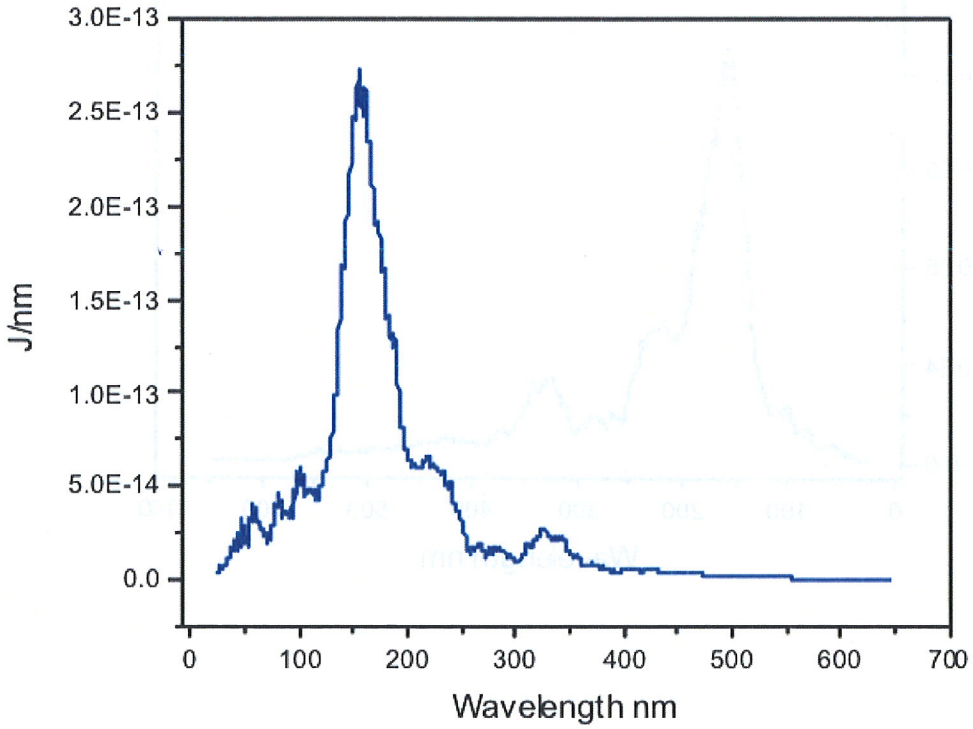

Figure 11. The wavelength calibrated and absolute intensity calibrated spectrum (22.8-647 nm) of the emission of hydrated silver shots comprising a source of H and HOH hydrino catalyst that were ignited by passing a low voltage, high current through the shot. The radiation is predominantly in the high-energy region with the predicted short wavelength emission of the H(1/4) continuum radiation.